Supplementary Materials

A novel structure Ti/Fe_2O_3/Cu_2S/$Co(OH)_x$ enhances the photoelectrochemical water splitting performance of iron oxide

Hao-Yan Shi[1,2,3], Yan-Xin Chen[1,2,3,4,*], Ming-Hao Ji[1,3], Qian-Qian Zhou[1,3], Ke-Xian Li[1,3], Hai-Long Wang[1,3], Rui Chen[1,3], Xiu-Mei Lin[5,*], Can-Zhong Lu[1,2,3,4,*]

[1]State Key Laboratory of Structural Chemistry, Fujian Institute of Research on the Structure of Matter, Chinese Academy of Sciences, Fuzhou 350002, Fujian, China.
[2]School of Chemical Sciences, University of Chinese Academy of Sciences, Beijing 100049, China.
[3]Xiamen Key Laboratory of Rare Earth Photoelectric Functional Materials, Xiamen Institute of Rare-earth Materials, Haixi Institutes, Chinese Academy of Sciences, Xiamen 361021, Fujian, China.
[4]Fujian Science & Technology Innovation Laboratory for Optoelectronic Information of China, Fuzhou 350108, Fujian, China.
[5]College of Chemistry, Chemical Engineering and Environment, Fujian Province University Key Laboratory of Analytical Science, Minnan Normal University, Zhangzhou 363000, Fujian, China.

[*]**Correspondence to:** Prof. Yan-Xin Chen, Prof. Can-Zhong Lu, State Key Laboratory of Structural Chemistry, Fujian Institute of Research on the Structure of Matter, Chinese Academy of Sciences, 155 Yangqiao Road West, Fuzhou 350002, Fujian, China. E-mail: yanxinchen@fjirsm.ac.cn; czlu@fjirsm.ac.cn; Dr. Xiu-Mei Lin, College of Chemistry, Chemical Engineering and Environment, Fujian Province University Key Laboratory of Analytical Science, Minnan Normal University, 36 Xianqian Street, Zhangzhou 363000, Fujian, China. E-mail: xiu-mei.lin@xmu.edu.cn

1. Supplementary Calculations

Generally, the turnover number (TON) for H_2 generation is defined as the ratio of reacting molecules to active sites, as shown in Equation S1.

$$TON = \frac{Number\ of\ reacted\ molecules}{Number\ of\ active\ sites} \quad (S1)$$

According to the review article by Xiaobo Chen et al.[1], the TON is usually used in molecular systems. However, evaluating semiconductor photocatalysts using Equation (1) is often difficult because their active sites cannot be accurately determined. Alternatively, the TON can be calculated using Equation S2 in semiconductor systems.

$$TON = \frac{Number\ of\ evolved\ H_2 \times 2}{Number\ of\ atoms\ in\ a\ photocatalyst} \quad (S2)$$

Clearly, the TON in Equation (2) is generally smaller than the real TON in Equation (1) due to the larger number of atoms compared to the number of real active sites.

The specific contents of Fe, Cu, and Co on the photoanode Ti/Fe_2O_3/Cu_2S/$Co(OH)_x$ were determined by ICP-MS. The final TON value for this photoanode after 3 hours of reaction was calculated as 1146 using Equation S3.

$$N = \frac{m}{\mathrm{M}}\mathrm{N_A} \quad (S3)$$

Here, N represents the number of atoms or molecules of the substance, m represents the mass of the substance, M represents the relative atomic mass of the element, and N_A represents Avogadro's constant.

The hole transport efficiency ($\eta_{surface}$) between the photoanode and the electrolyte was calculated to better illustrate the separation of charge carriers[2]. The $\eta_{surface}$ is described by the following Equation S4:

$$\eta_{surface} = \frac{J_{H_2O}}{J_{Na_2SO_3}} \quad (S4)$$

Here, J_{H_2O} represents the LSV test result of the photoelectrode in a 1 M KOH electrolyte, while $J_{Na_2SO_3}$ represents the LSV test result of the photoelectrode in a 1 M KOH + 1 M Na_2SO_3 electrolyte. Na_2SO_3 is added because SO_3^{2-} has a low activation energy and fast oxidation kinetics. This ensures that all photogenerated holes reaching the photoelectrode/electrolyte interface are immediately depleted, and surface charge recombination can be neglected. Thus, Na_2SO_3 is used as a hole-scavenging agent.

2. Supplementary Figures

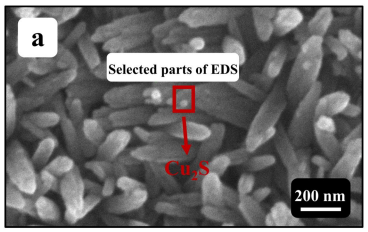

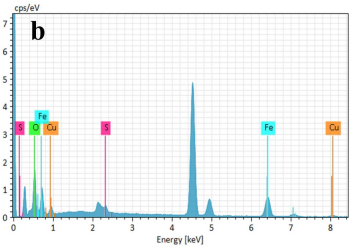

c

element	Quality(%)	Normalized quality(%)	Atom(%)
O	2.89	28.57	57.68
Fe	4.21	41.63	24.08
Cu	2.38	23.57	11.98
S	0.63	6.22	6.26
	10.10	100	100

Supplementary Figure 1. (a) SEM image of Cu_2S nanoparticles loaded on photoanode Ti/Fe_2O_3. (b) Distribution of elements in the selected parts of the EDS. (c) Elemental content map of selected parts of EDS. The samples with the best photoelectric properties had low Cu_2S content, which was difficult to see on the SEM. To prove that Cu_2S nanoparticles were loaded on the surface of Fe_2O_3, the loading of Cu_2S was increased to ensure that the Cu_2S nanoparticles could be seen on the SEM. EDS also proved the presence of the elements of Cu and S with a ratio of the atoms of the two of 2:1, which suggests that it is Cu_2S.

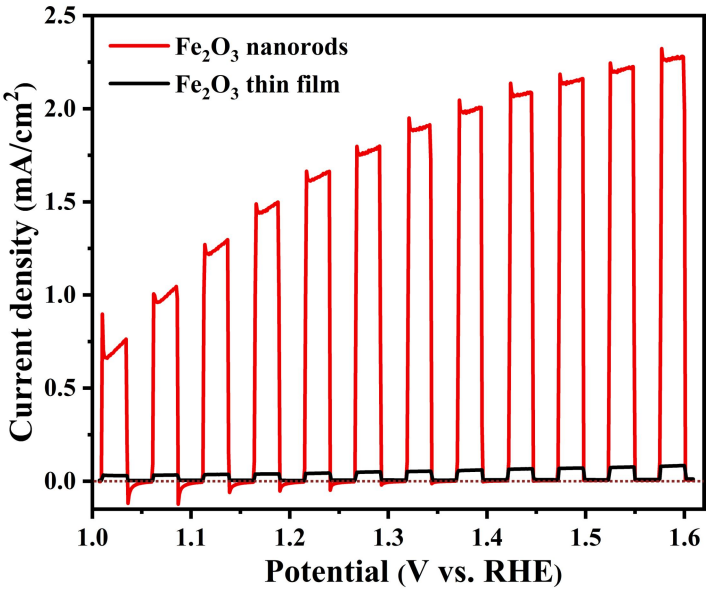

Supplementary Figure 2. LSV curves under AM 1.5G (light intensity: 100 mW/cm^2). Fe_2O_3 thin film was obtained by magnetron sputtering of an iron oxide target on a titanium sheet; Fe_2O_3 nanorods are the photoanode Ti/Fe_2O_3. Both were annealed at the same temperature. By testing, it can be found that the photocurrent of the iron oxide nanorods is significantly higher than that of the iron oxide films. This reflects the advantage of 1D morphology in observing high photocurrents.

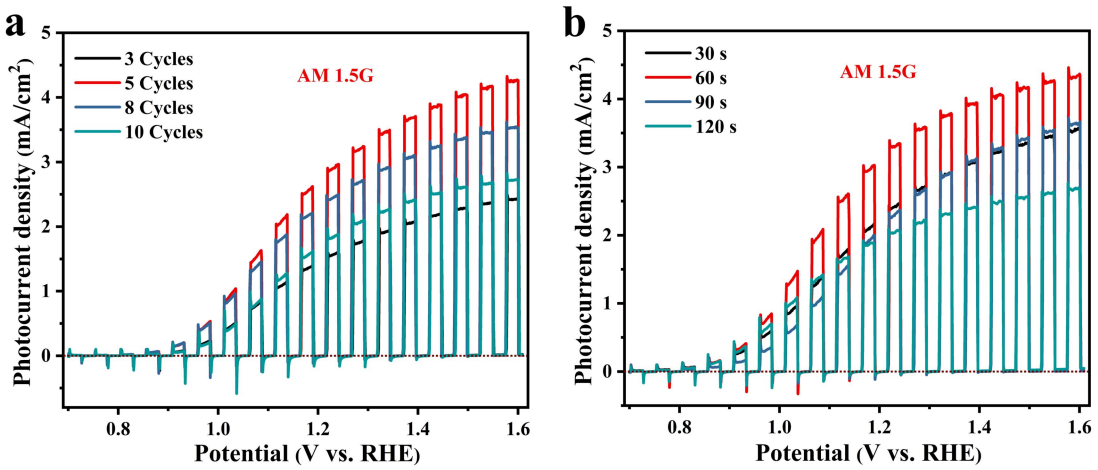

Supplementary Figure 3. LSV curves under AM 1.5G (light intensity: 100 mW/cm^2). (a) Influence of different Cu_2S contents on the Ti/Fe_2O_3 performance of photoanodes. (b) Influence of different $Co(OH)_x$ contents on the Ti/Fe_2O_3 performance of photoanodes.

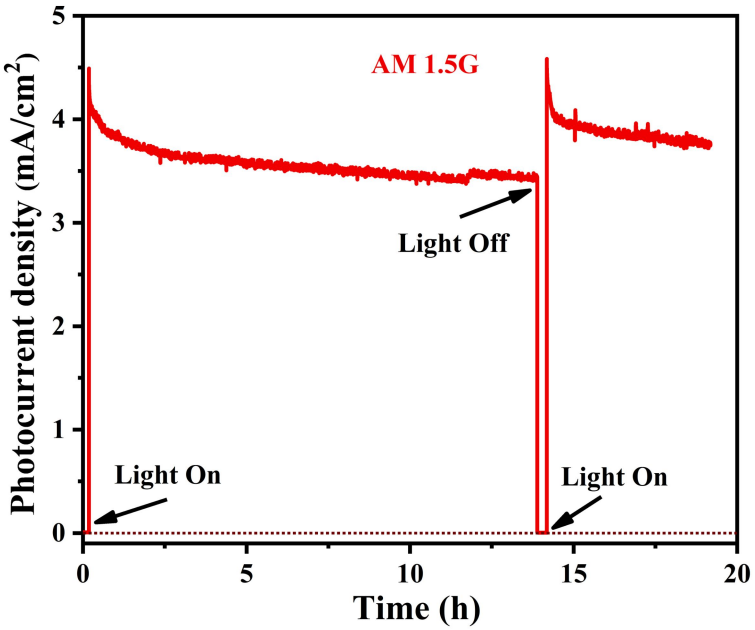

Supplementary Figure 4. Chronoamperometry data plots at 1.23 V *vs.* RHE. Stability test of photoanode Ti/Fe_2O_3/Cu_2S/$Co(OH)_x$.

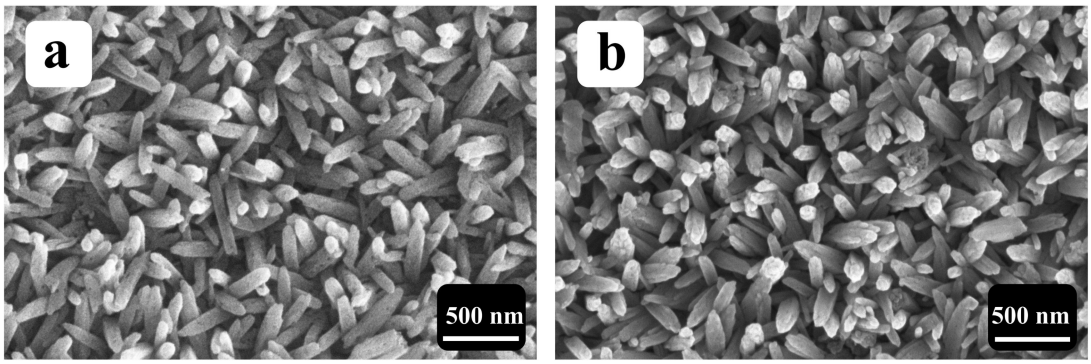

Supplementary Figure 5. (a) SEM image of photoanode Ti/Fe_2O_3/Cu_2S/$Co(OH)_x$ before stability testing; (b) SEM image of photoanode Ti/Fe_2O_3/Cu_2S/$Co(OH)_x$ after stability testing. Since the main component of the photoanode used in this work is Fe_2O_3, the amounts of Cu_2S and $Co(OH)_x$ are very small. Therefore, SEM mainly represents the properties of Fe_2O_3. As can be seen from Supplementary Figure 5, the morphology of the samples before and after the stability test remained consistent. These two features further prove the stability of the samples.

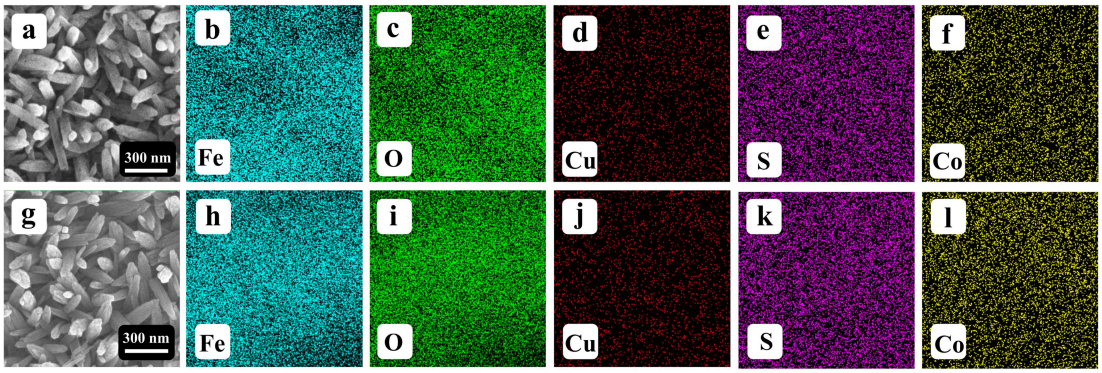

Supplementary Figure 6. (a) SEM image of photoanode Ti/Fe_2O_3/Cu_2S/$Co(OH)_x$ before stability testing; (b-f) EDS image of photoanode Ti/Fe_2O_3/Cu_2S/$Co(OH)_x$ before stability testing; (g) SEM image of photoanode Ti/Fe_2O_3/Cu_2S/$Co(OH)_x$ after stability testing; (h-i) EDS image of photoanode Ti/Fe_2O_3/Cu_2S/$Co(OH)_x$ after stability testing. EDS (Supplementary Figure 6) also proved the presence of several elements, namely Fe, O, Cu, S, and Co. Together, the above tests proved the stability of the sample properties.

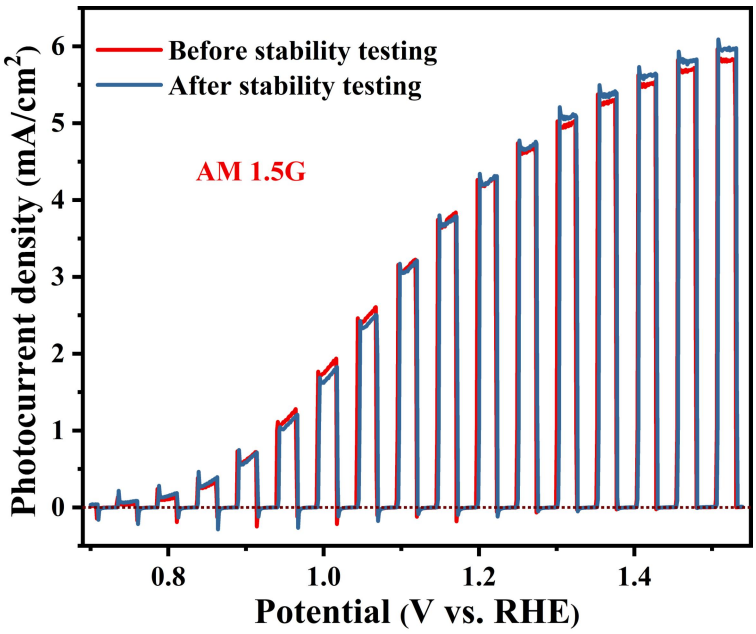

Supplementary Figure 7. LSV curves under AM1.5G (light intensity: 100 mW/cm^2). Comparison of LSV curves of photoanode Ti/Fe_2O_3/Cu_2S/$Co(OH)_x$ before and after stability tests. The results of the LSV test (Supplementary Figure 7) showed that the photocurrent values of the samples before and after the stability test were almost unchanged.

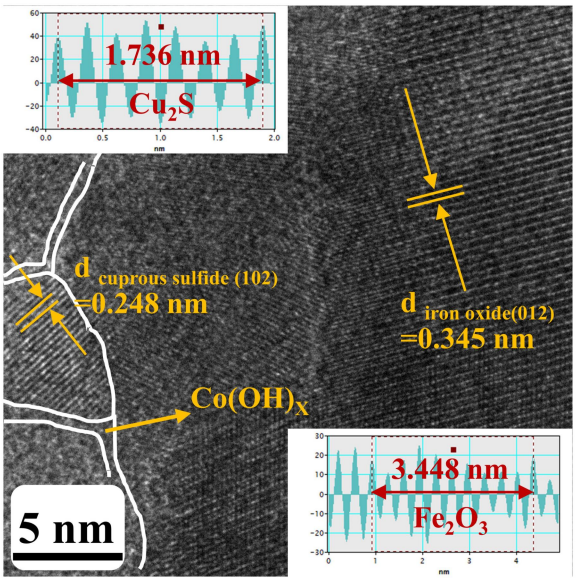

Supplementary Figure 8. The TEM images of the photoanode Ti/Fe_2O_3/Cu_2S/$Co(OH)_x$ after stability testing. The three-phase interface of Fe_2O_3, CuO, and $Co(OH)_x$ is also clearly visible in the TEM photographs.

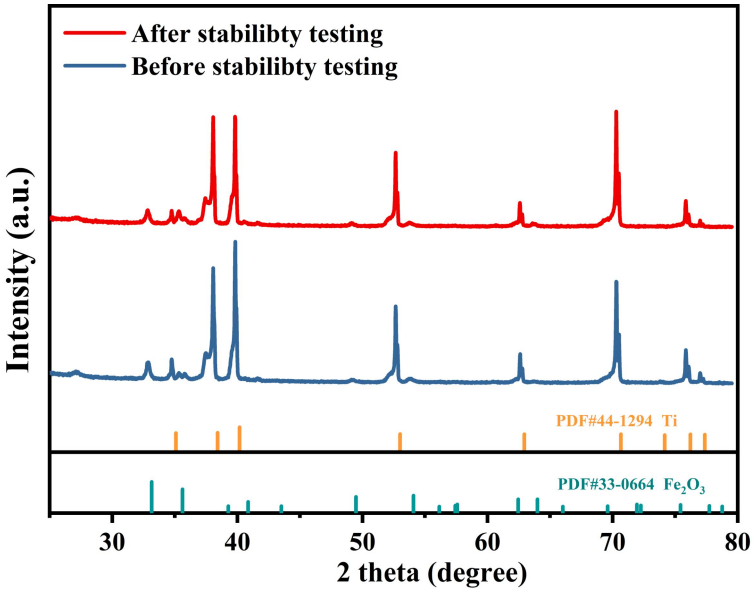

Supplementary Figure 9. XRD patterns of photoanode Ti/Fe_2O_3/Cu_2S/$Co(OH)_x$ before and after stability testing. The samples before and after the stability test performed XRD characterization, as shown in Supplementary Figure 9. As can be seen from Supplementary Figure 9, the XRD patterns of the samples before and after the stability test were almost unchanged.

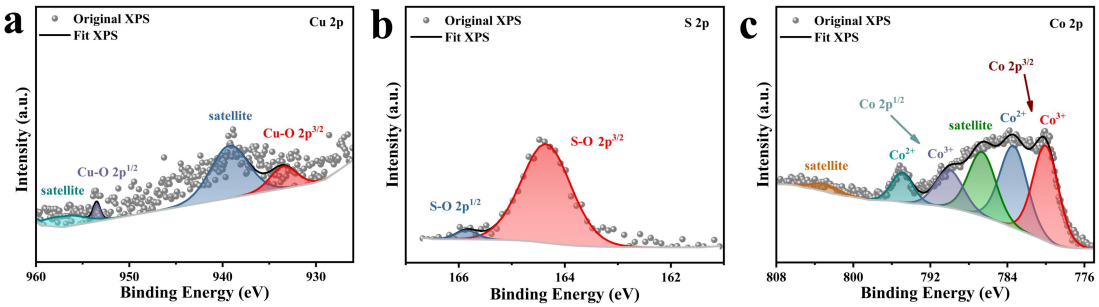

Supplementary Figure 10. XPS plots of photoanode Ti/Fe_2O_3/Cu_2S/$Co(OH)_x$ after stability testing. (a) Cu 2p; (b) S 2p; (c) Co 2p. XPS characterization (Figure S10) showed that Cu_2S was converted to CuO after the photocatalytic reaction (Figure 4D and Supplementary Figure 10a). Still, a significant portion of the S-O covalent bond was retained at the interface (Supplementary Figure 10b). As a reported[3] co-catalyst for water oxidation, the generated CuO can counteract the unfavorable effect of the conversion of Cu_2S to CuO on the photoelectrochemical process[4]. These results suggest that forming S-O chemical bonds between Cu_2S and Fe_2O_3 is essential for improving and stabilizing PEC performance. In addition, the XPS fitting results for Co 2p were similar before and after the photocatalytic reaction (Figure 4F and Supplementary Figure 10c), which suggests that the $Co(OH)_x$ material will not be oxidized to metal oxides. The results after stability tests further highlight the critical role of ultrathin $Co(OH)_x$ nanosheets in preventing photo corrosion and improving the performance of photoanode PEC.

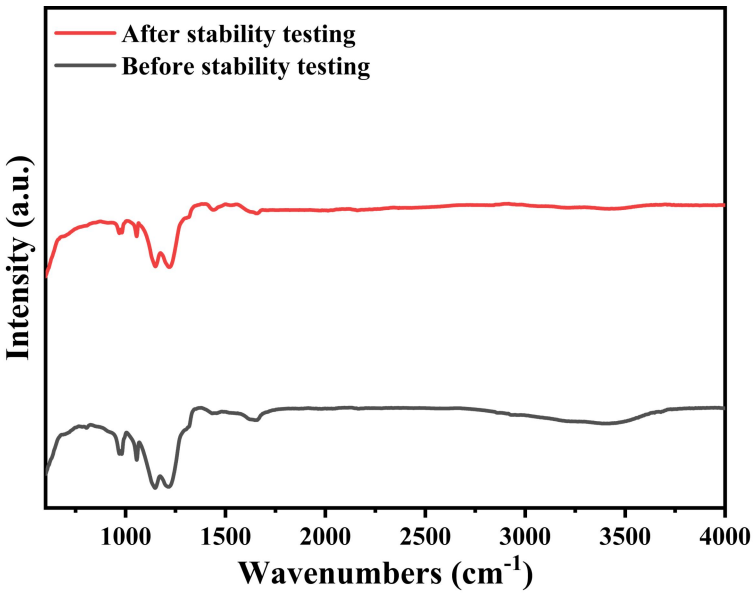

Supplementary Figure 11. FT-IR spectra of photoanode Ti/Fe_2O_3/Cu_2S/$Co(OH)_x$ before and after stability testing. As can be seen from Supplementary Figure 11, the FTIR spectra of the samples did not change significantly before and after the stability test.

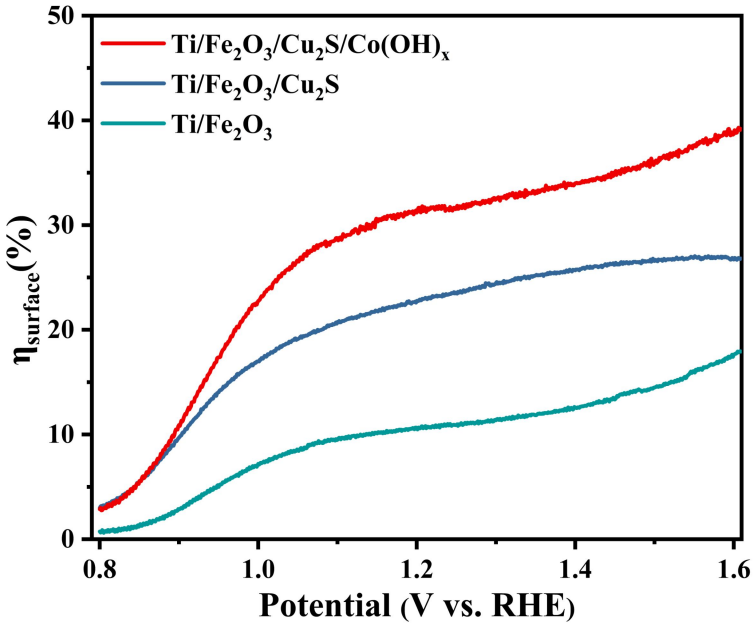

Supplementary Figure 12. $\eta_{surface}$ curves. The introduction of Cu_2S and $Co(OH)_x$ enhances the separation efficiency of photogenerated electrons and holes in Fe_2O_3, as depicted in Supplementary Figure 12. Conversely, the Ti/Fe_2O_3/Cu_2S/$Co(OH)_x$ photoanode exhibits the highest $\eta_{surface}$, indicating the lowest electron-hole conformity.

3. Supplementary Tables

Supplementary Table 1. Comparison of PEC performance of $Ti/Fe_2O_3/Cu_2S/Co(OH)_x$ photoanode with other reported Fe_2O_3-based photoanodes in this study.

Fe_2O_3-based photoanodes	Photocurrent density at 1.23 V (*vs.* RHE) (mA cm^{-2}, AM 1.5G, 100 mW cm^{-2})	Ref.
$Ta:Fe_2O_3@CaFe_2O_4$	2.7	[5]
$ZnFe_2O_4/Fe_2O_3$	3.17	[6]
$Fe_2O_3@Co_3O_4/GQDs$	3.63	[7]
$Fe_2O_3/Fe_2TiO_5/FeTi$-LDH	3.54	[8]
$Hf:Fe_2O_3@HfO_x/NiCoFe(OH)_x$	4.13	[9]
SAs $Pt:Fe_2O_3$-O_v	3.65	[10]
$NiFe(OH)_x/P_{Si}$/Ge-PH	4.57	[11]
Fe_2O_3/Ir	1.35	[12]
$Ti/Fe_2O_3/Cu_2S/Co(OH)_x$	4.8	This work

Supplementary Table 2. The fitting data of the equivalent circuit (Tested at 1.23V *vs.* RHE)

Sample	R_s (Ω)	R_1 (KΩ)	R_2 (KΩ)	R_3 (Ω)	CPE_1 (μF)	CPE_2 (μF)	C_1 (μF)	Z_w (KDW)
Ti/Fe_2O_3	44.5	2.99	140	1220	5.61	0.183	42.1	19.4
$Ti/Fe_2O_3/Cu_2S$	2.37	4.88	6.07	566	16.6	0.0633	103	3.21
$Ti/Fe_2O_3/Cu_2S/Co(OH)_x$	16.3	4.93	82.2	509	19.1	0.0793	72.4	2.5

Supplementary Table 3. The fitting data of the equivalent circuit (Tested at open circuit potential)

Sample	R_s (Ω)	R_1 (KΩ)	R_2 (KΩ)	R_3 (Ω)	CPE_1 (μF)	CPE_2 (μF)	C_1 (μF)	Z_w (KDW)
Ti/Fe_2O_3	1.21	5.55	87.7	624	18.6	0.059	122	8.75
$Ti/Fe_2O_3/Cu_2S$	2.03	5.79	2.95	603	18.2	0.063	953	0.9
$Ti/Fe_2O_3/Cu_2S/Co(OH)_x$	12.0	4.64	36.8	584	17.4	0.070	193	1.17

REFERENCES

1. Li X, Yu JG, Low JX, Fang YP, Xiao J, Chen XB. Engineering heterogeneous semiconductors for solar water splitting. *J Mater Chem A* 2015;3:2485-534. http://doi.org/10.1039/c4ta04461d.

2. Ji MH, Chen YX, Chen R, et al. A novel a-Fe_2O_3 photoanode with multilayered In_2O_3/Co-Mn nanostructure for efficient photoelectrochemical water splitting. *Int J Hydrogen Energy* 2024;51:66-77. http://doi.org/10.1016/j.ijhydene.2023.08.061.

3. Wang WZ, Wang J, Wang ZZ, et al. p-n junction CuO/$BiVO_4$ heterogeneous nanostructures: synthesis and highly efficient visible-light photocatalytic performance. *Dalton Trans* 2014;43:6735-43. http://doi.org/10.1039/c3dt53613k.

4. Li JQ, Cui MM, Guo ZY, Liu ZX, Zhu ZF. Synthesis of dumbbell-like CuO-$BiVO_4$ heterogeneous nanostructures with enhanced visible-light photocatalytic activity. *Mater Lett* 2014;130:36-39. http://doi.org/10.1016/j.matlet.2014.05.084.

5. Kang K, Tang C, Kim JH, et al. In situ construction of Ta:Fe_2O_3@$CaFe_2O_4$ core-shell nanorod p-t-n heterojunction photoanodes for efficient and robust solar water oxidation. *ACS Catal* 2023;13:7002-12. http://doi.org/10.1021/acscatal.3c00932.

6. Hu X, Huang J, Cao Y, et al. Photothermal-boosted polaron transport in Fe_2O_3 photoanodes for efficient photoelectrochemical water splitting. *Carbon Energy* 2023. http://doi.org/10.1002/cey2.369.

7. Li C, Ma S, Zhao M, Jing M, Yuan W, Li C. Self-Assembled α-Fe_2O_3@Co_3O_4/Graphene Quantum dot core-hybrid shell wormlike nanoarrays with synergistic effects for photoelectrochemical water oxidation. *ACS Sustainable Chem Eng* 2023;11:12102-13. http://doi.org/10.1021/acssuschemeng.3c02859.

8. Fouemina JCN, Li G, She X, et al. Surface self-transforming FeTi-LDH overlayer in Fe_2O_3/Fe_2TiO_5 photoanode for improved water oxidation. *Small* 2023. http://doi.org/10.1002/smll.202301114.

9. Li W, Guo H, Xu C, Tang C, Lee JS, Zhang H. Hole storage overlayer of amorphous hafnium oxide for boosting hematite-based solar water splitting. *Appl Catal B-Environ Energy* 2024;342. http://doi.org/10.1016/j.apcatb.2023.123465.

10. Gao R-T, Zhang J, Nakajima T, et al. Single-atomic-site platinum steers photogenerated charge carrier lifetime of hematite nanoflakes for photoelectrochemical water splitting. *Nat Commun* 2023;14. http://doi.org/10.1038/s41467-023-38343-6.

11. Ahn H-J, Yoon K-Y, Sung M, et al. Utilizing a siloxane-modified organic semiconductor for photoelectrochemical water splitting. *ACS Energy Lett* 2023;8:2595-602. http://doi.org/10.1021/acsenergylett.3c00755.
12. Yuan S-Y, Jiang LW, Hu J-S, Liu H, Wang J-J. Fully dispersed IrO_X atomic clusters enable record photoelectrochemical water oxidation of hematite in acidic media. *Nano Lett* 2023;23:2354-61. http://doi.org/10.1021/acs.nanolett.3c00245.